Advances in Chemical Engineering and Science, 2014, 4, 374-388
Published Online July 2014 in SciRes. http://www.scirp.org/journal/aces
http://dx.doi.org/10.4236/aces.2014.43041

Synthesis, Structural and Photophysical Properties of $Gd_2O_3:Eu^{3+}$ Nanostructures Prepared by a Microwave Sintering Process

Ana P. de Moura[1], Larissa H. Oliveira[1], Içamira C. Nogueira[2], Paula F. S. Pereira[1], Máximo S. Li[3], Elson Longo[1], José A. Varela[1], Ieda L. V. Rosa[4*]

[1]Chemistry Institute, State University of Sao Paulo-UNESP, Araraquara, Brazil
[2]Department of Engineering Materials, Federal University of Sao Carlos, São Carlos, Brazil
[3]Institute of Physics of São Carlos, USP, São Carlos, Brazil
[4]Department of Chemistry, Federal University of Sao Carlos, São Carlos, Brazil
Email: [*]ilvrosa@ufscar.br

Received 17 June 2014; revised 7 July 2014; accepted 17 July 2014

Abstract

In this paper, we report the obtention of gadolinium oxide doped with europium ($Gd_2O_3:Eu^{+3}$) by thermal decomposition of the $Gd(OH)_3:Eu^{3+}$ precursor prepared by the microwave assisted hydrothermal method. These systems were analyzed by thermalgravimetric analyses (TGA/DTA), X-ray diffraction (XRD), structural Rietveld refinement method, fourrier transmission infrared absorbance spectroscopy (FT-IR), field emission scanning electron microscopy (FE-SEM) and photoluminescence (PL) measurement. XRD patterns, Rietveld refinement analysis and FT-IR confirmed that the $Gd(OH)_3:Eu^{3+}$ precursor crystallize in a hexagonal structure and space group *P6/m*, while the $Gd_2O_3:Eu^{3+}$ powders annealed in range of 500˚C and 700˚C crystallized in a cubic structure with space group Ia-3. FE-SEM images showed that $Gd(OH)_3:Eu^{3+}$ precursor and $Gd_2O_3:Eu^{3+}$ are composed by aggregated and polydispersed particles structured as nanorods-like morphology. The excitation spectra consisted of an intense broad band with a maximum at 263 nm and the Eu^{3+} ions can be excited via matrix. The emission spectra presented the characteristics $^5D_0 \rightarrow {}^7F_{0,1,2,3 \text{ and } 4}$ transitions of the Eu^{3+} ion, whose main emission, $^5D_0 \rightarrow {}^7F_2$, is observed at 612 nm. The photophysical properties indicated that the microwave sintering treatment favored the Eu^{3+} ions connected to the O-Gd linkages in the Gd_2O_3 matrix. Also, the emission in the $Gd_2O_3:Eu^{3+}$ comes from the energy transfered from the Gd-O linkages to the $[EuO_8]^{\bullet}$ clusters in the crystalline structure.

[*]Corresponding author.

How to cite this paper: de Moura, A.P., *et al*. (2014) Synthesis, Structural and Photophysical Properties of $Gd_2O_3:Eu^{3+}$ Nanostructures Prepared by a Microwave Sintering Process. *Advances in Chemical Engineering and Science*, **4**, 374-388.
http://dx.doi.org/10.4236/aces.2014.43041

Keywords

Gadolinuim Oxide, Europium Luminescence, Nanorods

1. Introduction

One-dimensional nanomaterials, such as nanotubes, nanowires, nanobelts or nanoribbons have attracted much interest in the past decade due to their physical properties and potential applications in nanotechnology fields [1]-[8]. Moreover, these materials can be applied as displays, catalysts, biological sensing, and other optoelectronic devices [9]-[11].

The demand for efficiency and high resolution waveguides, lamps and other optical devices has also stimulated the discovery of new luminescent materials with superior properties. Thus, there has been a tremendous interest in the subject of materials science for the development of new luminescent materials. The improved performance of display requires high-quality phosphors for sufficient brightness and long-term stability. To enhance the luminescent characteristics of phosphors, extensive research has been carried out on rare-earth activated oxide phosphors due to their superiority in color purity, chemical and thermal stabilities [12]-[14]. In this context, lanthanide hydroxides and oxides have actively been investigated for its application in multilayered capacitors, luminescent lamps and displays, solid-laser devices, optoelectronic data storages, waveguides, and heterogeneous catalysts. Their composition, structure and particle size depend on the synthesis method. Moreover, the chemical homogeneity and morphology of the synthesized products determine the effectiveness of their properties [11] [15] [16]. When they are applied for a fluorescent labeling, for instance, there are several advantages such as sharp emission spectra, long lifetimes, and high resistance against photobleaching in comparison with conventional organic fluorophores and quantum dots [17]-[19].

In particular, the gadolinium oxide doped with Eu^{3+} (Gd_2O_3:Eu^{3+}) exhibits a strong paramagnetic behavior (S 1/4 72) as well as strong UV and cathode-rays have also been observed in the lanthanide (Sm^{3+}, Er^{3+}) doped Gd_2O_3 excited luminescence, which are useful in biological fluorescent label, contrast agent, and display applications [20]-[22]. In addition, Gd_2O_3:Eu^{3+} is a very efficient X-ray and thermo-luminescent phosphor [23].

Europium ion in a trivalent state is one of the most studied rare earth element because of the simplicity of its emission spectra and due to the wide application as red phosphor in color TV screens. Eu^{3+} *f-f* transitions are sensitive to its local environment. The monitoring of different concentrations of the Eu^{3+} content into a ceramic material is very interesting in understanding the nature of the lattice modifiers as well as the degree of order-disorder into its crystalline structure. The most intense *f-f* transition is the $^5D_0 \rightarrow {}^7F_2$ transition at 616 nm. When this ion is presented in a non-centrosymmetric site, it can be used as an activator ion with red emission which has been used in the most commercial red phosphor. Moreover, the intensity of Eu^{3+} excitations at around 394 and 465 nm is improved in these materials as compared with most other Eu^{3+} doped phosphors [24] [25]. Because of it, this ion is able to be applied as biological sensors, phosphors, electroluminescent devices, optical amplifiers or lasers when it is used as a dopant in a variety of ceramic materials [26]-[28].

A variety of preparation methods have been developed to reduce the reaction temperature and achieve a small particle size of high quality Gd_2O_3:Eu^{3+} phosphors [11] [29]-[32].

Microwave heat processing has been successfully applied for the preparation of micro or nanosized inorganic materials [33]-[38]. The microwave-assisted heating is a greener approach to synthesize materials in a shorter time (from several minutes to a few hours) and with lower power consumption (hundreds of Watts) compared to the conventional heating at the same temperatures [39]-[43]. This is a consequence of directly and uniformly heating of the components, and exchange in the reaction selectivity, which can increase the reactional rates (microwave catalysis). Consequently, microwave synthesis is becoming quite common in several material sciences areas, nanotechnology, inorganic, organic, biochemical, or pharmaceutical laboratories [44]-[50].

In the present work, we investigated the photo-physical properties of Gd_2O_3: Eu^{3+} phosphors obtained by the thermal decomposition in range of 500˚C and 700˚C of the $Gd(OH)_3$:Eu^{3+} precursor prepared by the microwave assisted hydrothermal method. These materials were structured and microstructurally analyzed by means of X-ray diffraction (XRD), Rietveld refinement method, fourrier transmission infrared absorbance spectroscopy (FT-IR), field emission scanning electron microscopy (FE-SEM). The photo-physical properties were investigated through the excitation and emission spectra of the Eu^{3+} ion as well as lifetime measurements.

2. Experimental Procedure

2.1. Synthesis of the Precursors

The synthesis of the precursors was performed using the following procedure: In a typical synthesis, 1.8 g of Gd_2O_3 and 0.018 g of Eu_2O_3 were dissolved in 3.0 mL of the HNO_3 solution. After the formation of a clear solution, this solution was kept under constant heating until complete evaporation of the acid. Then 80 mL of distilled water were added to the solution and stirred for 30 min at room temperature. After that, an aqueous KOH (2.0 M) solution was added until the pH of solution was adjusted to be in the range of 12 giving rise to a colloidal precipitates. After stirring for about 30 min, the resultant solution was transferred to a Teflon lined stainless autoclave. This autoclave was then sealed and placed into a microwave system (MH) using 2.45 GHz microwave radiation with maximum power of 800 W. The MH conditions were kept at 140˚C for 1 minute. The white powders obtained ($Gd(OH)_3:Eu^{3+}$) were collected, washed with water and ethanol, and then dried at 60˚C for 8 h under atmospheric air in a conventional furnace.

2.2. Synthesis of $Gd_2O_3:Eu^{3+}$ Powders

The $Gd_2O_3:Eu^{3+}$ powders were obtained from thermal decomposition of the $Gd(OH)_3:Eu^{3+}$ precursors. These precursor powders were placed in ceramic crucibles and heated in a microwave sintering furnace at 500˚C, 550˚C, 600˚C, 650˚C and 700˚C for 5 min under an ambient atmosphere using a heating rate of 5˚C/min producing white powders denoted as $Gd_2O_3:Eu^{3+}$.

2.3. Characterization

The $Gd(OH)_3:Eu^{3+}$ and $Gd_2O_3:Eu^{3+}$ powders were structurally characterized by X-ray diffraction (XRD) in normal routine and Rietveld routine using a Rigaku-DMax/2500PC (Japan) with Cu-Kα radiation (λ = 1.5406 Å) and in the 2θ range from 10˚ to 130˚ with a scanning rate of 0.02˚/min. Fourier Transmission Infrared absorbance spectroscopy (FT-IR) analysis were taken in a FT-IR Bruker model EQUINOX spectrophotometer in range of 500 and 4000 cm^{-1}. Crystals morphologies were verified using a Scanning Electron Microscope (Jeol JSM-6460LV microscope). Photoluminescence (PL) was measured with a Thermal Jarrel-Ash Monospec 27 monochromator and a Hamamatsu R446 photomultiplier. The 350.7 nm exciting wavelength of a krypton ion laser (Coherent Innova) was used, with the nominal output power of the laser power kept at 200 mW. All the measurements were taken at room temperature. The excitation and emission spectra of the $Gd_2O_3:Eu^{3+}$ powders were measured in a Jobin Yvon-Fluorolog 3 spectrofluorometer at room temperature using a 450 W xenon lamp as excitation energy source. Lifetime data of the Eu^{3+} $^5D_0 \rightarrow {}^7F_2$ (λ_{exc} = 394 nm, λ_{em} = 612 nm) transition in the $Gd_2O_3:Eu^{3+}$ samples were evaluated from the decay curves using the emission wavelength set at 612 nm and excitation wavelength set at 393 nm.

3. Results and Discussion

3.1. Thermogravimetric Analyses (TGA/DTA)

Figure 1 presents the TGA curve of the as-prepared $Gd(OH)_3:Eu^{3+}$ powder. It can be seen in this figure, during the MH process, the thermal degradation of the $Gd(OH)_3:Eu^{3+}$ powders occurs in a two-step process in accordance to observed by Chang *et al*. [51]. The first-step occurs at 436˚C, where a weight loss of 8.3% is reported, while the second-step, occurs from 436˚C to 700˚C, a weight loss of 3.3% is revealed. From these results, it was confirmed that the MH treatments of the hydroxide precursor give rise to a stable $Gd_2O_3:Eu^{3+}$ matrix at temperatures up to 400˚C. Moreover, the two-step dehydration process indicates the presence of an intermediate phase in addition to the starting hexagonal $Gd(OH)_3:Eu^{3+}$ and the final cubic $Gd_2O_3:Eu^{3+}$. The theoretical weight loss of each process in this work is in a good agreement with shown by the literature.

3.2. X-Ray Diffraction (XRD) and Rietveld Refinement Analyses

XRD patterns of the as-prepared $Gd(OH)_3:Eu^{3+}$ are presented in **Figure 2(A)**, where the reflectance peaks of a

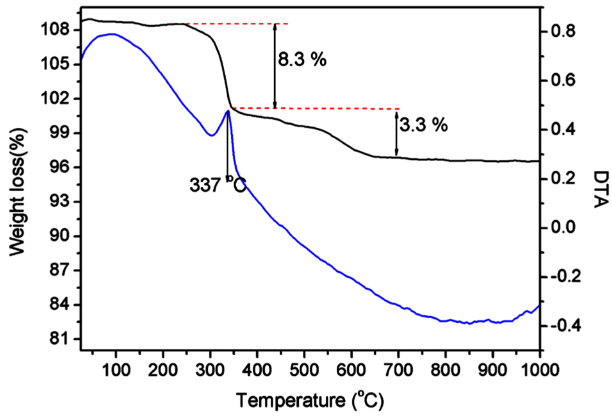

Figure 1. TGA/DTA curves of the as prepared $Gd(OH)_3:Eu^{3+}$.

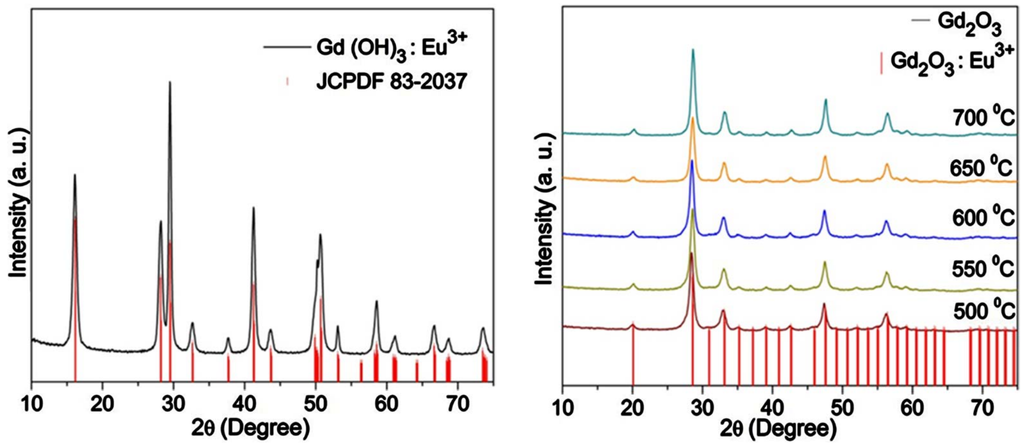

(A) (B)

Figure 2. (A) XRD patterns of $Gd(OH)_3:Eu^{3+}$ precursor obtained by the MH conditions at 140˚C for 1 min. (B) XRD patterns of $Gd_2O_3:Eu^{3+}$ powders prepared by thermal decomposition of the precursor $Gd(OH)_3:Eu^{3+}$.

pure hexagonal $Gd(OH)_3:Eu^{3+}$ phase with space group *P*63*/m* can be perfectly indexed in agreement with the respective Inorganic Crystal Structure Database (ICSD) card number 200,093. After the thermal decomposition of the $Gd(OH)_3:Eu^{3+}$ in range of 500˚C to 700˚C for 5 min (**Figure 2(B)**), it was observed that all the samples can be perfectly indexed to the cubic structure of crystalline Gd_2O_3 and space group Ia-3 (ICSD # 94892). None secondary phases were detected in these samples, indicating that all the $Gd(OH)_3:Eu^{3+}$ precursor heated from 500˚C to 700˚C giving rise to $Gd_2O_3:Eu^{3+}$ powders. In addition, in this range of temperature, any significant change in the XRD peak profiles of the $Gd_2O_3:Eu^{3+}$ samples were detected.

To better analyze the influence of the precursor thermal decomposition, the $Gd(OH)_3:Eu^{3+}$ and $Gd_2O_3:Eu^{3+}$ powders were submitted to the Rietveld refinement analysis.

The Rietveld refinement is a method in which the profile intensities obtained from step-scanning measurements of the powders allow to estimate an approximate structural model for the real structure [52]. In our work, the Rietveld refinement was performed using the General Structure Analysis (GSAS) program [53]. In these analyses, the parameters like scale factor, background, shift lattice constants, profile half-width parameters (u, v, w), isotropic thermal parameters, strain anisotropy factor, occupancy and atomic functional positions were refined. The background was corrected using a Chebyschev polynomial of the first kind. The peak profile function was modeled using a convolution of the Thompson-Cox-Hastings pseudo-Voigt (pV-TCH) [54] with asymmetry function described by Finger *et al*. [55]. To account for the anisotropy in the half width of the reflections, it was used the model proposed by Stephens [56].

The obtained results from the Rietveld refinement analyses of the crystalline $Gd(OH)_3:Eu^{3+}$ and $Gd_2O_3:Eu^{3+}$

are shown in **Figure 3**. The results showed that the $Gd(OH)_3:Eu^{3+}$ powder crystallize in a hexagonal structure, space group *P*63*/m* and two clusters per unit cell (Z = 2), while the $Gd_2O_3:Eu^{3+}$ powders crystallize in a cubic structure, space group Ia-3 and sixteen formula units per cell (Z = 16). These results showed a good relation between the observed XRD patterns and the theoretical ones, as shown by a line ($Y_{obs} - Y_{cal}$) at **Figure 3**. Moreover, it was not verified the presence of secondary phases related to the Eu^{3+} ions, probably indicating that these ions were incorporated to the hydroxide and oxide matrixes. The lattice parameters, unit cell volume, unit cell angles and correlation parameters (R_{Bragg}, χ^2 and R_{wp}) obtained by means of the structural refinement data for analyzed powders are listed in **Table 1** and **Table 2**.

From the lattice parameters, unit cell volume and atomic positions obtained from the Rietveld refinement data, it was possible to model a schematic representation of the hexagonal $Gd(OH)_3:Eu^{3+}$ unit cell and space group *P*63/*m* **Figure 4(A)**, using the Visualization for Electronic and Structural Analysis (VESTA) program version 2.1.6 for Windows [57].

In the literature, the crystalline structure of the $Gd(OH)_3$ has been studied by Chang *et al.* [51]. From this schematic representation is was possible to observed that the hexagonal $Gd(OH)_3$ is composed by $[Gd(OH)_3]^-$

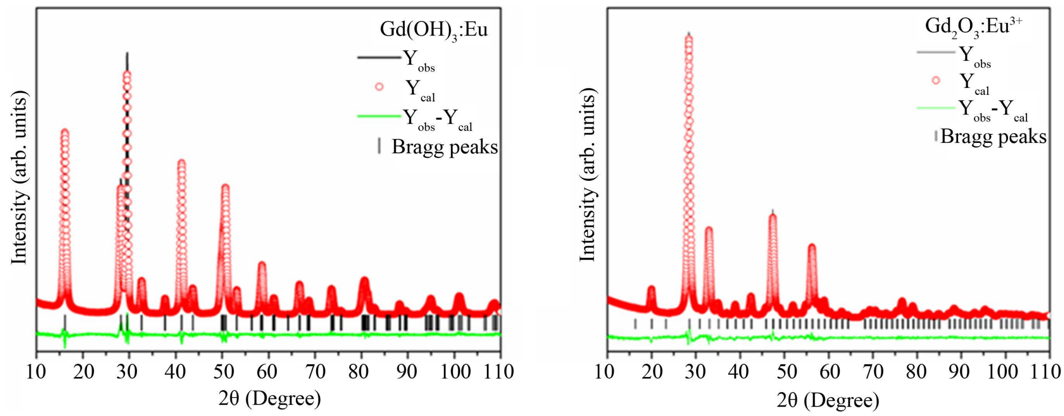

Figure 3. Rietveld refinement data for the $Gd(OH)_3:Eu^{3+}$ and $Gd_2O_3:Eu^{3+}$ powders, respectively.

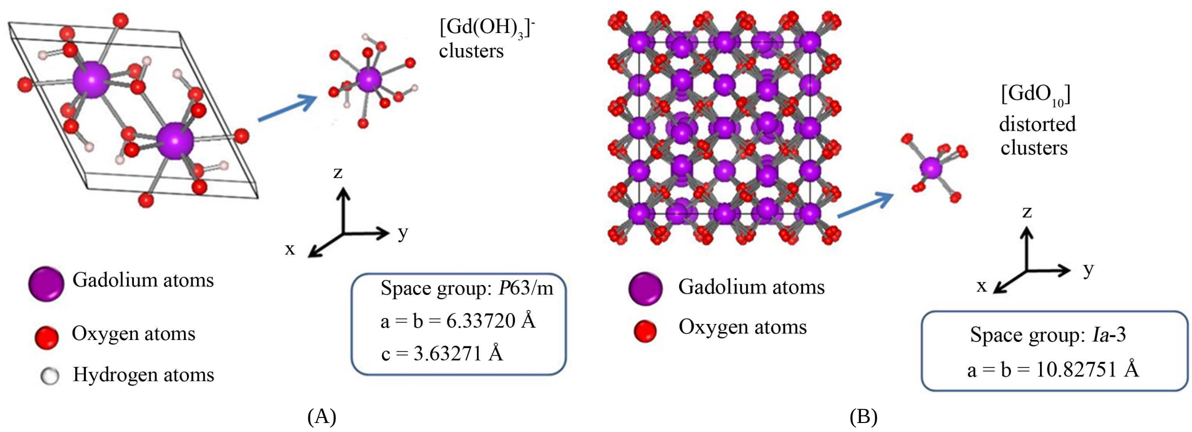

Figure 4. Schematic representation of the $Gd(OH)_3:Eu^{3+}$ (A) and $Gd_2O_3:Eu^{3+}$ (B) unit cell, respectively.

Table 1. Lattice parameters, unit cell volume of $Gd(OH)_3:Eu^{3+}$ obtained by MH processing at 140˚C for 1 min.

	Lattice Parameters		Cell volume ($Å^3$)	Unit cell angle (˚)		R_{Bragg} (%)	χ^2 (%)	R_{wp} (%)	R_p (%)
	a, *b* (Å)	*c* (Å)		*α* = *β*	□				
$Gd(OH)_3:Eu^{3+}$	6.337 (2)	3.632 (7)	126.344 (4)	90	120	2.80	1.98	6.38	5.08
ICSD # 200093	6.329 (2)	3.631 (1)	125.960	90	120	-	-	-	-

Table 2. Lattice parameters, unit cell volume of $Gd_2O_3:Eu^{3+}$ obtained by thermal decomposition of the $Gd(OH)_3:Eu^{3+}$ precursor at 700˚C.

	Lattice parameters (Å)	Cell volume (Å^3)	Unit cell angle (˚)	R_{Bragg} (%)	χ^2 (%)	R_{wp} (%)	R_p (%)
	$a = b = c$		$\alpha = \beta = \gamma$				
$Gd_2O_3:Eu^{3+}$	10.82751 (22)	126.344 (4)	90	2.93	1.70	6.46	5.01
ICSD # 94892	10.82311 (20)	126.782	90	-	-	-	-

clusters connected to each other. Moreover, the addition of Eu^{3+} in its crystalline structure promotes the expansion of the $Gd(OH)_3$ unit cell as a consequence of the substitution of some Gd sites by the Eu ion ones.

The unit cell of the $Gd_2O_3:Eu^{3+}$ powder was also simulated through the VESTA software and its schematic representation is illustrated at **Figure 4(B)**. From this schematic representation the $Gd_2O_3:Eu^3$ are composed by the Gd atoms coordinated to ten oxygen atoms forming $[GdO_{10}]$ clusters which are connected to each other and all dispersed to the cubic crystalline structure, which are in good agreement with References [58] and [59].

From **Table 2**, it can be seen any significant changes in lattice parameters (*a*, *b* and *c*) of Gd_2O_3 system as function of the heat treatment. When the $Gd(OH)_3:Eu^{3+}$ material is subjected to a thermal treatment in a microwave oven sintering, there is an interaction of the Gd, O and H atoms with the microwave radiation in the crystalline structure. Consequently, the heating of these systems occurs. This process is able to promote the dehydration of the $Gd(OH)_3:Eu^{3+}$ material giving rise to Gd_2O_3 crystalline structure. Due to low heating rate used (5˚C /min), this interaction occurs slowly and the quantity of surface defects is reduced as well as particle growth is promoted [60].

3.3. Fourier Transmission Infrared Absorption Spectroscopy (FT-IR)

Figure 5 shows the FT-IR transmission spectra of the $Gd(OH)_3:Eu^{3+}$ precursor and of the $Gd_2O_3:Eu^{3+}$ nanocrystals obtained heated at 500˚C, 550˚C, 600˚C, 650˚C and 700˚C for 5 min.

The FT-IR of the $Gd(OH)_3:Eu^{3+}$ precursor presents a sharp absorption band at 3610 cm^{-1} which is characteristic of the Gd-OH matrix. The bands at around 3460 and 1627 cm^{-1} are due to the OH stretching (υ) and OH deformation vibrations (δ), respectively. The broad at absorptions around 2333 cm^{-1} is assigned to the existence of CO_2. The absorption bands at around 1480 and 400 cm^{-1} are ascribed to the CO asymmetric vibration (υ_{as}).

The sharp peak observed for the $Gd(OH)_3:Eu^{3+}$ precursors is ascribed to the OH stretching vibration, and indicates the absence of hydrogen bonds between the hydroxyls group [61]. Thus, it can be supposed that the $[Gd(OH)_3]^-$ clusters in the $Gd(OH)_3$ are connected to each other, in accordance to the Rietveld refinement analysis. In the IR absorption spectra of the $Gd_2O_3:Eu^{3+}$ powders annealed from 500˚C to 700˚C, it was observed the appearance of some absorption at around 525 and 830 cm^{-1} characteristic of Gd-O vibrations, confirming the formation of an oxide matrix after the heat treatment process [62] [63]. Also, the broad absorption bands observed at 3460 cm^{-1} in these samples are only corresponded to the water absorbed in its superficies. All these results are also in agreement with the Rietveld refinement analysis.

The intensity of the absorption bands corresponding to the OH and CO groups are strong dependent of the annealing temperature, indicating that the powder prepared in air atmosphere have strong absorption to water and CO_2 and it can be potentially applied as gas sensors in monitoring gases such as water and CO_2.

3.4. Field Emission Scanning Electron Microscopy (FE-SEM)

Figure 6 shows the FE-SEM images of the $Gd(OH)_3:Eu^{3+}$ precursor (A) and $Gd_2O_3:Eu^{3+}$ samples heated at 500˚C (B), 550˚C (C), 600˚C (D), 650˚C (E) and 700˚C (F), respectively. The FE-SEM images showed that the $Gd_2O_3:Eu^{3+}$ and $Gd(OH)_3:Eu^{3+}$ powders are composed by aggregated and polydispersed particles structured as nanorods-like morphology. Moreover, the size and thickness of the $Gd_2O_3:Eu^{3+}$ powders (**Figures 6(B)-(F)**) vary as function of the annealing temperature. It was also noticed that as the temperature increases the particles have a tendency to agglomerate.

FE-SEM images were also employed to evaluate the average particle size distribution (width) of the $Gd(OH)_3:Eu^{3+}$ and $Gd_2O_3:Eu^{3+}$ nanostructures. During this measurement was considered around 100 nanostructures and the best fit for this system was adjusted as a lognormal function, which is described by the following equation:

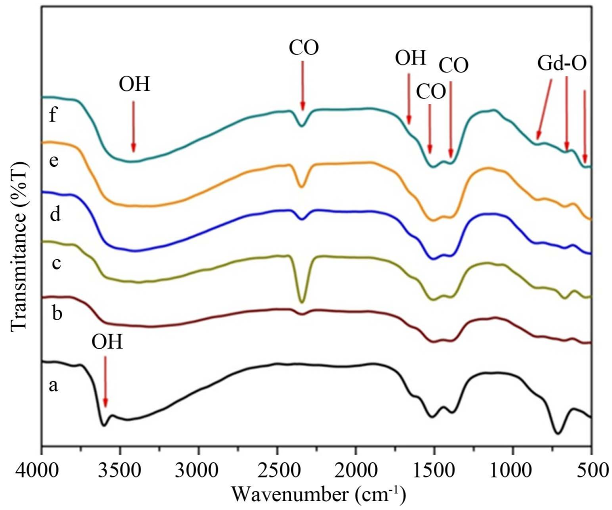

Figure 5. FE-SEM images of $Gd(OH)_3:Eu^{3+}$ precursor (A) and $Gd_2O_3:Eu^{3+}$ samples heat at 500˚C (B), 550˚C (C), 600˚C (D), 650 ˚C (E) and 700˚C (F), respectively.

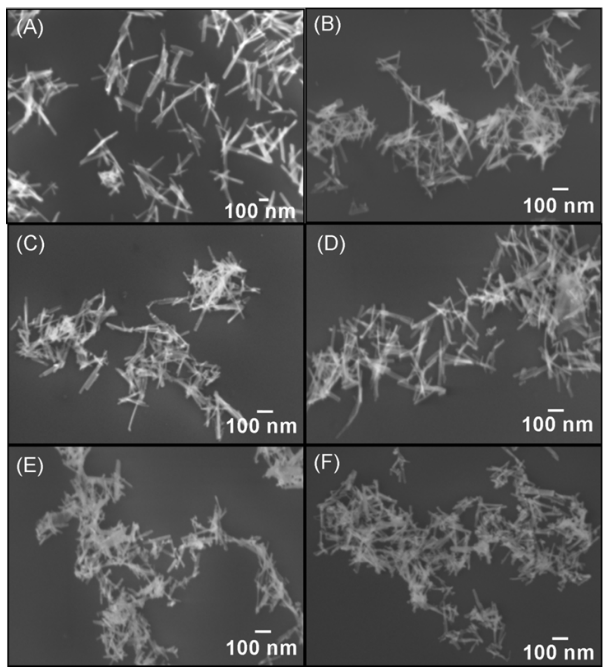

Figure 6. Average thickness distribution of $Gd(OH)_3:Eu^{3+}$ precursor (A) and $Gd_2O_3:Eu^{3+}$ samples heat at 500˚C (B), 550˚C (C), 600˚C (D), 650˚C (E) and 700˚C (F), respectively.

$$Y = Y_0 + \frac{A}{\sqrt{2\pi WX}} \mathrm{e}^{\frac{-\left[\ln \frac{x}{xc}\right]^2}{2w^2}} \tag{1}$$

where y_0 is the first value in y-axis, A is the amplitude, w is the width, π is a constant, x_c is the center value of the distribution curve in x-axis.

The obtained results shown in **Figure 7** presented an assymmetrical distribution on the logarithmic scale of average particle size. In this case, it was noted that almost all particles presented an average width between 8 and 20 nm.

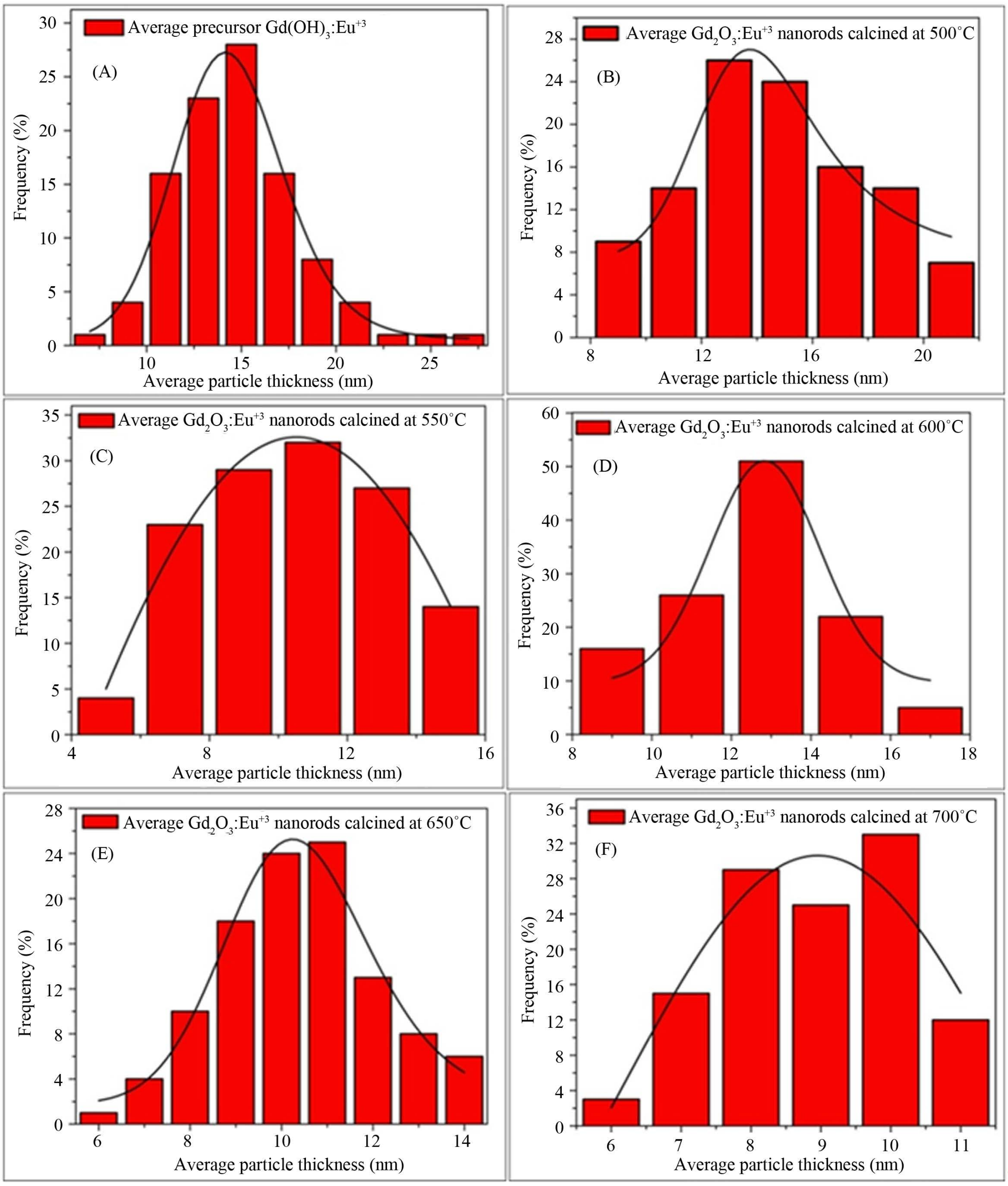

Figure 7. FT-IR spectra of the $Gd(OH)_3:Eu^{3+}$ precursor (A) and of the $Gd_2O_3:Eu^{3+}$ calcined at: 500˚C (B); 550˚C (C); 600˚C (D); 650 ˚C (E) and 700˚C (F).

3.5. Photoluminescence (PL) Emission Measurements

Figure 8(A) illustrates the PL spectra of the $Gd(OH)_3:Eu^{3+}$ precursor and $Gd_2O_3:Eu^{3+}$ samples heat treated at 500˚C, 550˚C, 600˚C, 650˚C and 700˚C, respectively and (B) the PL spectrum of the non-doped Gd_2O_3 prepared by the microwave assisted hydrothermal method. All the measurements were recorded at room temperature.

To a better understanding of the PL properties and its dependence on the structural order-disorder in the Gd_2O_3 lattice, the PL emission spectra of the $Gd(OH)_3:Eu^{3+}$ and $Gd_2O_3:Eu^{3+}$ powders were performed at room temperature, using an excitation of a krypton laser source at 350.7 nm. **Figure 8(A)** also shows a broad emission band from 400 to 600 nm. This band can be ascribed to the emission of the Gd_2O_3 matrix as it was confirmed by the PL emission spectrum of Gd_2O_3 powder where a broad band with maximum situated at 449 nm were observed (**Figure 8(B)**). Moreover, in range of 600 and 700 nm, it was possible to noticed the intra-configurational

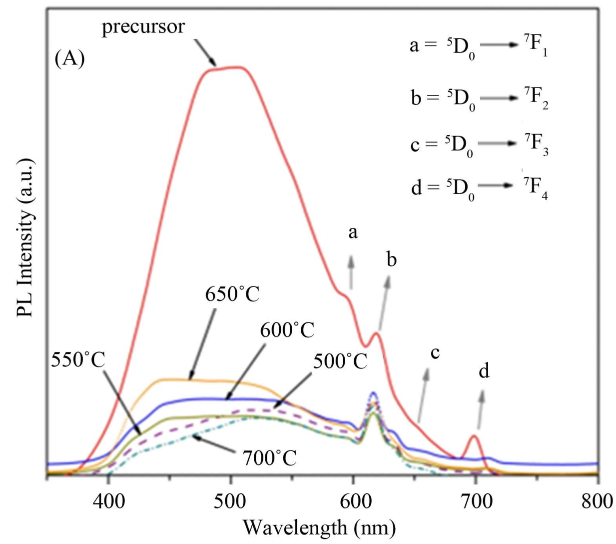

(A)

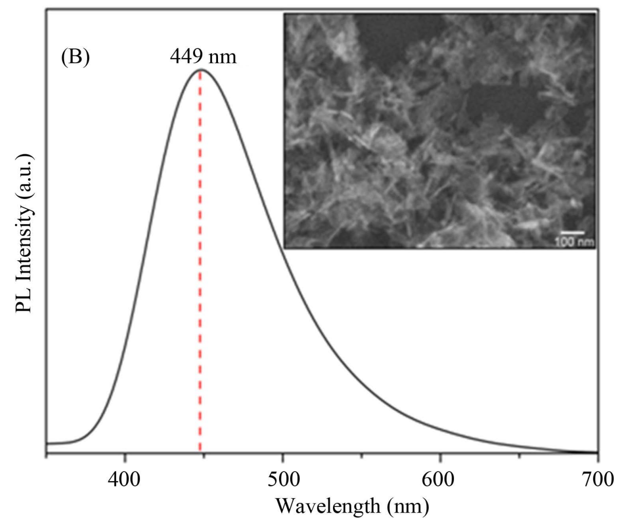

(B)

Figure 8. PL emission spectra of the $Gd(OH)_3:Eu^{3+}$ and $Gd_2O_3:Eu^{3+}$ powders heated in different temperatures (A) and pure Gd_2O_3 heat treated at 600˚C. Insert: FE-SEM image of pure Gd_2O_3 powder.

$4f_6$ transitions of the Eu^{3+} ions specifically the $^7F_0 \rightarrow {}^5D_J$ (J = 1, 2, 3 and 4) transitions at 590, 615, 633 and 710 nm, respectively, for all analyzed samples.

Figure 9 shows the excitation spectra of $Gd_2O_3:Eu^{3+}$ powders annealed at 500˚C, 550˚C, 600˚C, 650˚C and 700˚C. The excitation spectra were recorded monitoring the emission wavelength at 612 nm. It can be clearly seen that the excitation spectra consist of a main intense broad band with a maximum at 263 nm attributed to the the $O^{2-} \rightarrow Eu^{3+}$ energy transfer state [64]-[67] and the internal Gd^{3+} $S^8 \rightarrow {}^6I$ and $^8S \rightarrow {}^6P$ transitions situated at 274 and 311 nm, respectively. These transitions are possible to be detected as a consequence of the $Gd^{3+} \rightarrow Eu^{3+}$ energy transfer [65] [66] in the Gd_2O_3 matrix (CTB). Above 330 nm, it was noted the Eu^{3+} $^4f_6$ intra-configurational transitions from the ground state $^7F_0$ to the excited states $^5G_6$ at 362 nm, $^5H_4$ at 380 nm, $^5L_6$ at 393 nm, $^5D_2$ at 464 nm and $^5D_1$ at 532 nm, respectively (**Figure 9**). In this case, we observed that the Eu^{3+} ion can be excited via matrix in a wide range of wavelength and the most intense absorption band is correspondent to the $S^8 \rightarrow {}^6I$ transition of the Gd^{2+} ions at 263 nm. Moreover, as the temperature increases the relative intensity of the bands corresponding to its transitions also increases [68].

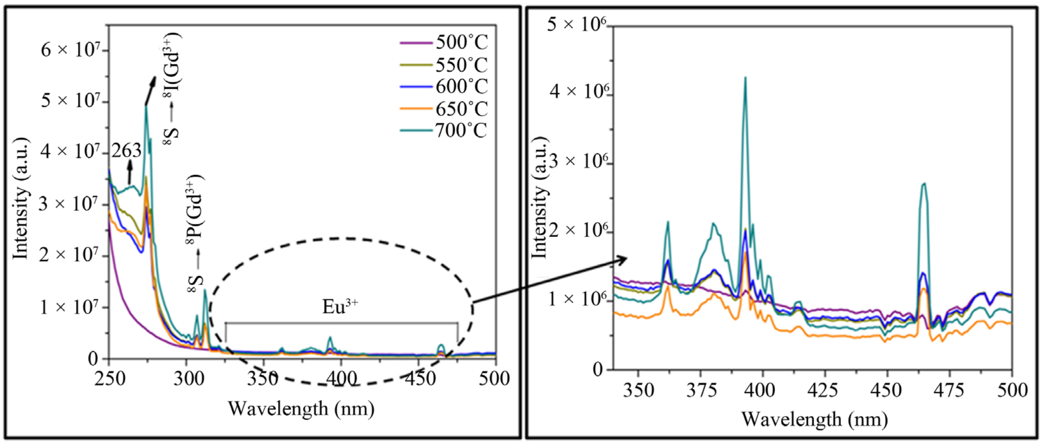

Figure 9. Excitation spectra of $Gd_2O_3:Eu^{3+}$ samples heated at 500˚C, 550˚C, 600˚C, 650˚C and 700˚C, λ_{em} = 612 nm.

The emission spectra of $Gd_2O_3:Eu^{3+}$ for the samples annealed at 500˚C, 550˚C, 600˚C, 650˚C and 700˚C are shown in **Figure 10**. These spectra were obtained setting the excitation wavelength into the energy transfer band CTB of Eu^{3+} at 263 nm.

The emission spectra of the Eu^{3+} ion present narrow bans ascribed to the ${}^5D_0 \rightarrow {}^7F_{0,1,2,3\text{ and }4}$ transitions at around 578, 589, 614, 652 and 699 nm, respectively. The most intense band is related to ${}^5D_0 \rightarrow {}^7F_2$ transition with maximum situate at 612 nm. The hypersensitive transition ${}^5D_0 \rightarrow {}^7F_2$ is dependent on the local Eu^{3+} environment due to its electric dipole character, while the intensity of ${}^5D_0 \rightarrow {}^7F_2$, a magnetic dipole transition is almost independent of the Eu^{3+} surroundings. Thus, the ratio ${}^5D_0 \rightarrow {}^7F_2/{}^5D_0 \rightarrow {}^7F_1$ emission intensity gave us valuable information about the environmental changes around the rare earth ions and can be used as a dimension of the degree of distortion from the inversion symmetry of the Eu^{3+} site in the lattice [69].

The ratio ${}^5D_0 \rightarrow {}^7F_2/{}^5D_0 \rightarrow {}^7F_1$ values obtained for the $Gd_2O_3:Eu^{3+}$ powders annealed at 500˚C, 550˚C, 600˚C, 650˚C and 700˚C is of 18.0, 17.1, 15.8, 11.95 and 18.3, respectively. The decrease in the ratio ${}^5D_0 \rightarrow {}^7F_2/{}^5D_0 \rightarrow {}^7F_1$ values as the temperature increases from 500˚C to 650˚C is a indicative that the Eu^{3+} ions is occupying higher symmetry sites. In this case, we believe that some Eu^{3+} is already connected to the –OH linkages from the $Gd(OH)_3$ precursor. However, there is an increase of the ratio ${}^5D_0\rightarrow{}^7F_2/{}^5D_0\rightarrow{}^7F_1$ value at 700˚C, indicating that now the Eu^{3+} ions is occupying lower symmetric sites. The temperature favored the higher symmetric coordination sites, since there is Eu^{3+} ions linked to the O-Gd linkages in the Gd_2O_3 matrix. Some of these oxygen atoms are in the first coordination sphere of Eu^{3+} ions giving rise to $[EuO_8]^\bullet$ clusters in this powder.

All these results indicates that probably the emission in the $Gd_2O_3:Eu^{3+}$ powders annealed from 500˚C to 700˚C comes from the energy transfer from the Gd-O linkages to the $[EuO_8]^\bullet$ clusters in the crystalline structure. Moreover, the increase of the relative intensity of the Eu^{3+} ${}^5D_0 \rightarrow {}^7F_{0,1,2,3\text{ and }4}$ transitions is strongly related to the formation of these complex clusters in the Gd_2O_3 matrix. The photoluminescence decay curves and lifetime of the Eu^{3+} ${}^5D_0 \rightarrow {}^7F_2$ transition with emission and excitation wavelengths set at 612 nm and 263 nm, respectively. In this work, the lifetime value of the $Gd_2O_3:Eu^{3+}$ samples as a function of the annealing temperatures are shown in **Figure 11**. All these curves can be fitted into a single exponential function as $I = I_0 \exp(-t/\tau)$ were (τ is the lifetime of the rare earth ion).

According to these data, it was observed that the lifetime of Eu^{3+} increases as the annealing temperature increases. This behavior is probably due to the increase of the energy transfer from the Gd-O linkages to the $[EuO_8]^\bullet$ clusters. All these results are in accordance to the emission and excitation measurements.

4. Conclusion

In summary, the obtained results showed that the $Gd(OH)_3:Eu^{3+}$ (precursor) was synthesized by the microwave assisted hydrothermal method in a short period of time (30 minutes). After heated treated from 500˚C to 700˚C,

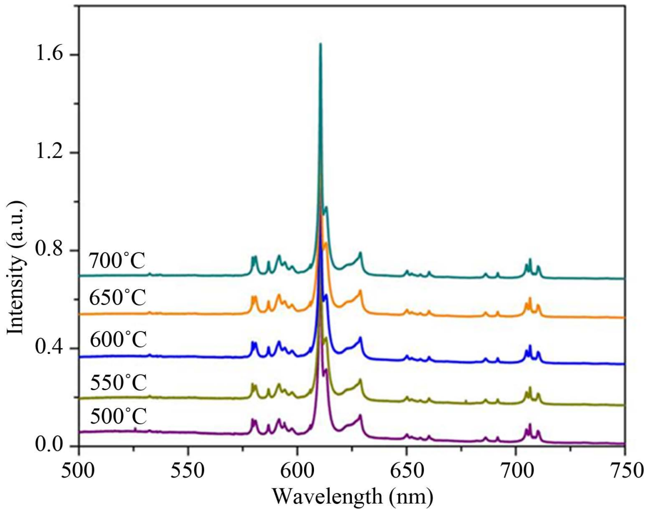

Figure 10. Emission spectra of $Gd_2O_3:Eu^{3+}$ samples calcined at 500˚C, 550˚C, 600˚C, 650˚C and 700˚C, λ_{ex} = 263 nm.

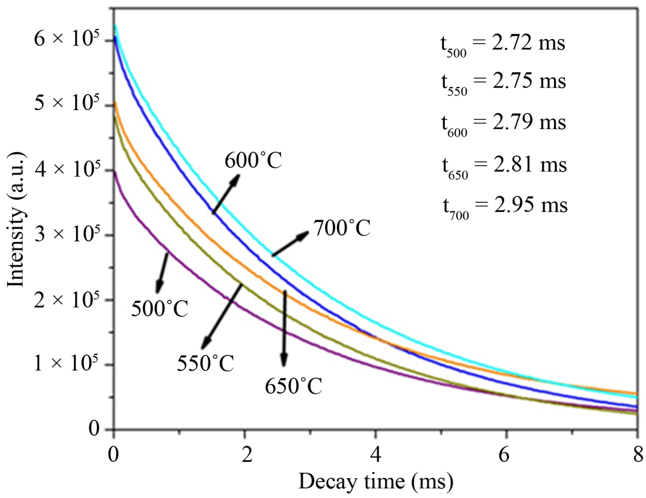

Figure 11. Decay curves and lifetime of the $^5D_0 \rightarrow {}^7F_2$ transition characteristic of the Eu^{3+} of the $Gd_2O_3:Eu^{3+}$ nanorods heat treated at 500˚C, 550˚C, 600˚C, 650˚C and 700˚C (λ_{ex} = 612 nm and λ_{em} = 612 nm).

the XRD patterns and Rietveld refinement and FT-IR analyses indicated the formation of $Gd_2O_3:Eu^{3+}$ powders which crystallizes in a cubic structure of crystalline Gd_2O_3 and space group Ia-3. No secondary phases related to the Eu^{3+} ions were detected indicating that these ions were incorporated to the hydroxide and oxide matrixes in the analyzed powders. FE-SEM images indicated that the $Gd(OH)_3:Eu^{3+}$ precursor and $Gd_2O_3:Eu^{3+}$ powders are composed by several aggregated particles with nanorods-like morphology, which sizes are in the range of 8 and 20 nm. Eu^{3+} emission and excitation spectra pointed out that the emission in the $Gd_2O_3:Eu^{3+}$ powders comes from the energy transfer from the Gd-O and $[EuO_8]^{\bullet}$ clusters in the crystalline structure. Moreover, these are in accordance to the lifetime values, which presented an increase as the temperature increases. This method is very simple and effective, and can be extended to synthesize some other rare earth and metal oxide nanorods.

Acknowledgements

The authors acknowledge the financial support of the Brazilian research financing institutions: CNPq (INCTMN), CAPES and FAPESP (CEPID). A special thanks for Maria Fernanda Cgnin de Abreu.

References

[1] Iijima, S. (1991) Synthesis of Carbon Nanotubes. *Nature*, **354**, 56-58. http://dx.doi.org/10.1038/354056a0

[2] Ajayan, P.M. (1999) Nanotubes from Carbon. *Chemical Reviews*, **99**, 1787-1800. http://dx.doi.org/10.1021/cr970102g

[3] Hu, J.T., Odom, T.W. and Lieber, C.M. (1999) Chemistry and Physics in one Dimension: Synthesis and Properties of Nanowires and Nanotubes. *Accounts of Chemical Research*, **32**, 435-445. http://dx.doi.org/10.1021/ar9700365

[4] Xia, Y.N., Yang, P.D., Sun, Y.G., Wu, Y.Y., Mayers, B., Gates, B., Yin, Y.D., Kim, F. and Yan, H.Q. (2003) One-Dimensional Nanostructures: Synthesis, Characterization, and Applications. *Advanced Materials*, **15**, 353-389. http://dx.doi.org/10.1002/adma.200390087

[5] Rao, C.N.R., Deepak, F.L., Gundiah, G. and Govindaraj, A. (2003) Inorganic Nanowires. *Progress in Solid State Chemistry*, **31**, 5-147. http://dx.doi.org/10.1016/j.progsolidstchem.2003.08.001

[6] Huang, M.H., Mao, S., Feick, H., Yan, H.Q., Wu, Y.Y., Kind, H., Weber, E., Russo, R., Yang, P.D. (2001) Room-Temperature Ultraviolet Nanowire Nanolasers. *Science*, **292**, 1897-1899. http://dx.doi.org/10.1126/science.1060367

[7] Pan, Z.W., Dai, Z.R. and Wang, Z.L. (2001) Nanobelts of Semiconducting Oxides. *Science*, **291**, 1947-1949. http://dx.doi.org/10.1126/science.1058120

[8] Shi, W.S., Peng, H., Wang, N., Li, C.P., Xu, L., Lee, C.S., Kalish, R. and Lee, S.T. (2001) Free-Standing Single Crystal Silicon Nanoribbons. *Journal of the American Chemical Society*, **123**, 11095-11096. http://dx.doi.org/10.1021/ja0162966

[9] Hu, J., Odom, T.W. and Lieber, C.M. (1999) Chemistry and Physics in One Dimension: Synthesis and Properties of Nanowires and Nanotubes. *Accounts of Chemical Research*, **32**, 435-445. http://dx.doi.org/10.1021/ar9700365

[10] Kazes, M., Lewis, D.Y., Ebenstein, Y., Mokari, T. and Banin, U. (2002) Lasing from Semiconductor Quantum Rods in a Cylindrical Microcavity. *Advanced Materials*, **14**, 317-321. http://dx.doi.org/10.1002/1521-4095(20020219)14:4<317::AID-ADMA317>3.0.CO;2-U

[11] Lee, K.-H., Bae, Y.-J. and Byeon, S.-H. (2008) pH Dependent Hydrothermal Synthesis and Photoluminescence of Gd_2O_3:Eu Nanostructures. *Bulletin of the Korean Chemical Society*, **29**, 2161-2168. http://dx.doi.org/10.5012/bkcs.2008.29.11.2161

[12] Ropp, R.C. (1993) The Chemistry of Artificial Lighting Devices: Lamps, Phosphors, and Cathode Ray Tubes. Elsevier, New York.

[13] Blasse, G. and Grabmaier, B.C. (1994) Luminescent Materials. Springer, New York. http://dx.doi.org/10.1007/978-3-642-79017-1

[14] Wan, J., Wang, Z., Chen, X., Mu, L. and Qian, Y. (2005) Shape-Tailored Photoluminescent Intensity of Red Phosphor Y_2O_3:Eu^{3+}. *Journal of Crystal Growth*, **284**, 538-543. http://dx.doi.org/10.1016/j.jcrysgro.2005.07.040

[15] Xu, G.X. and Xiao, J.M. (1985) New Frontiers Rare Earth Science and Application. Academic Press, New York.

[16] Cuif, J.P., Rohart, E., Macaudiere, P., Bauregard, C., Suda, E., Pacaud, B., Imanaka, N., Masui, T. and Tamura, S. (2004) Binary Rare Earth Oxides. Kluwer Academic Publishers, Dordrecht.

[17] Bae, Y.J., Lee, K.H. and Byeon, S.H. (2009) Synthesis and Eu^{3+} Concentration-Dependent Photoluminescence of $Gd_{2-x}Eu_xO_3$ Nanowires. *Journal of Luminescence*, **129**, 81-85. http://dx.doi.org/10.1016/j.jlumin.2008.08.004

[18] Beaurepaire, E., Buissette, V., Sauviat, M.P., Mercuri, A., Martin, J.L., Lahlil, K., Aume, D., Huignard, A., Gacoin, T., Boilot, J.P. and Alexandrou, A. (2004) Functionalized Fluorescent Oxide Nanoparticles: Artificial Toxins for Sodium Channel Targeting and Imaging at the Single-Molecule Level. *Nano Letters*, **4**, 2079-2083. http://dx.doi.org/10.1021/nl049105g

[19] Louis, C., Bazzi, R., Marquette, C.A., Bridot, J.L., Roux, S., Ledoux, G., Mercier, B., Blum, L., Perriat, P. and Tillement, O. (2005) Nanosized Hybrid Particles with Double Luminescence for Biological Labeling. *Chemistry of Materials*, **17**, 1673-1682. http://dx.doi.org/10.1021/cm0480162

[20] Nichkova, M., Dosev, D., Gee, S.J., Hammock, B.D. and Kennedy, I.M. (2005) Quantum Dots as Reporters in Multiplexed Immunoassays for Biomarkers of Exposure to Agrochemicals. *Analytical Letters*, **40**, 1423-1433.

[21] Goldys, E.M., Tomsia, K.D., Jinjun, S., Dosev, D., Kennedy, I.M., Yatsunenko, S. and Godlewski, M. (2006) Optical Characterization of Eu-Doped and Undoped Gd_2O_3 Nanoparticles Synthesized by the Hydrogen Flame Pyrolysis Method. *Journal of the American Chemical Society*, **128**, 14498-14505. http://dx.doi.org/10.1021/ja0621602

[22] Zhou, Y., Lin, J. and Wang, S. (2003) Energy Transfer and Up-Conversion Luminescence Properties of Y_2O_3:Sm and Gd_2O_3:Sm Phosphors. *Journal of Solid State Chemistry*, **171**, 391-395. http://dx.doi.org/10.1016/S0022-4596(02)00219-0

[23] Rossner, W. and Grabmaier, B.C. (1991) Phosphors for X-Ray Detectors in Computed Tomography. *Journal of Luminescence*, **48-49**, 29-36. http://dx.doi.org/10.1016/0022-2313(91)90072-4

[24] Guo, C., Chen, T., Luan, L., Zhang, W. and Huang, D. (2008) Luminescent Properties of $R_2(MoO_4)_3:Eu^{3+}$ (R = La, Y, Gd) Phosphors Prepared by Sol-Gel Process. *Journal of Physics and Chemistry of Solids*, **69**, 1905-1911. http://dx.doi.org/10.1016/j.jpcs.2008.01.021

[25] Pereira, P.F.S., de Moura, A.P., Nogueira, I.C., Lima, M.V.S., Longo, E., de Sousa Filho, P.C., Serra, O.A., Nassar, E.J. and Rosa, I.L.V. (2012) Study of the Annealing Temperature Effect on the Structural and Luminescent Properties of $SrWO_4$:Eu Phosphors Prepared by a Non-Hydrolytic Sol-Gel Process. *Journal of Alloys and Compounds*, **526**, 11-21. http://dx.doi.org/10.1016/j.jallcom.2012.02.083

[26] Rosa, I.L.V., Oliveira, L.H., Suzuki, C.K., Varela, J.A., Leite, E.R. and Longo, E. (2008) SiO_2-GeO_2 Soot Perform as a Core for Eu_2O_3 Nanocoating: Synthesis and Photophysical Study. *Journal of Fluorescence*, **18**, 541-545. http://dx.doi.org/10.1007/s10895-007-0297-7

[27] Morais, E.A., Scalvi, L.V.A., Tabata, A., De Oliveira, J.B.B. and Ribeiro, S.J.L. (2008) Photoluminescence of Eu^{3+} Ion in SnO_2 Obtained by Sol-Gel. *Journal of Materials Science*, **43**, 345-349. http://dx.doi.org/10.1007/s10853-007-1610-1

[28] Marques, A.P.A., Tanaka, M.T.S., Longo, E., Leite, E.R. and Rosa, I.L.V. (2011) The Role of the Eu^{3+} Concentration on the $SrMoO_4$:Eu Phosphor Properties: Synthesis, Characterization and Photophysical Studies. *Journal of Fluorescence*, **21**, 893-899. http://dx.doi.org/10.1007/s10895-010-0604-6

[29] Yan, M.F., Huo, T.C.D. and Ling, H.C.J. (1987) Preparation of $Y_3Al_5O_{12}$-Based Phosphor Powders. *Journal of the Electrochemical Society*, **134**, 493-498. http://dx.doi.org/10.1149/1.2100487

[30] Shea, L.E., McKittrick, J., Lopez, O.A. and Sluzky, E. (1996) Synthesis of Red-Emitting, Small Particle Size Luminescent Oxides Using an Optimized Combustion Process. *Journal of the American Ceramic Society*, **79**, 3257-3265. http://dx.doi.org/10.1111/j.1151-2916.1996.tb08103.x

[31] Ravichandran, D., Roy, R., White, W.B. and Erdei, S. (1997) Synthesis and Characterization of Sol-Gel Derived Hexa-Aluminate Phosphor. *Journal of Materials Research*, **12**, 819-824. http://dx.doi.org/10.1557/JMR.1997.0119

[32] Erdei, S., Roy, R., Harshe, G., Juwhari, S., Agrawal, H.D., Ainger, F.W. and White, W.B. (1995) The Effect of Powder Preparation Processes on the Luminescent Properties of Yttrium Oxide Based Phosphor Materials. *Materials Research Bulletin*, **30**, 745-753. http://dx.doi.org/10.1016/0025-5408(95)00052-6

[33] Santos, M.L., Lima, R.C., Riccardi, C.S., Tranquilin, R.L., Bueno, P.R., Varela, J.A. and Longo, E. (2008) Preparation and Characterization of Ceria Nanospheres by Microwave-Hydrothermal Method. *Materials Letters*, **62**, 4509-4511. http://dx.doi.org/10.1016/j.matlet.2008.08.011

[34] Lima, R.C., Macario, L.R., Espinosa, J.W.M., Longo, V.M., Erlo, R., Marana, N.L., Sambrano, J.R., Santos, M.L.D., Moura, A.P., Pizani, P.S., Andres, J., Longo, E. and Varela, J.A. (2008) Toward an Understanding of Intermediate- and Short-Range Defects in ZnO Single Crystals. A Combined Experimental and Theoretical Study. *The Journal of Physical Chemistry A*, **112**, 8970-8978. http://dx.doi.org/10.1021/jp8022474

[35] Moura, A.P., Cavalcante, L.S., Sczancoski, J.C., Stroppa, D.G., Paris, E.C., Ramirez, A.J., Varela, J.A. and Longo, E. (2010) Structure and Growth Mechanism of CuO Plates Obtained by Microwave-Hydrothermal without Surfactants. *Advanced Powder Technology*, **21**, 197-202. http://dx.doi.org/10.1016/j.apt.2009.11.007

[36] de Moura, A.P., Lima, R.C., Moreira, M.L., Volanti, D.P., Espinosa, J.W.M., Orlandi, M.O., Pizani, P.S., Varela, J.A. and Longo, E. (2010) ZnO Architectures Synthesized by a Microwave-Assisted Hydrothermal Method and Their Photoluminescence Properties. *Solid State Ionics*, **181**, 775-780. http://dx.doi.org/10.1016/j.ssi.2010.03.013

[37] Motta, F.V., Lima, R.C., Marques, A.P.A., Li, M.S., Leite, E.R., Varela, J.A. and Longo, E. (2010) Indium Hydroxide Nanocubes and Microcubes Obtained by Microwave-Assisted Hydrothermal Method. *Journal of Alloys and Compounds*, **497**, L25-L28. http://dx.doi.org/10.1016/j.jallcom.2010.03.069

[38] de Moura, A.P., Lima, R.C., Paris, E.C., Li, M.S., Varela, J.A. and Longo, E. (2011) Formation of β-Nickel Hydroxide Plate-Like Structures under Mild Conditions and Their Optical Properties. *Journal of Solid State Chemistry*, **184**, 2818-2823.

[39] Bohr, H. and Bohr, J. (2000) Microwave-Enhanced Folding and Denaturation of Globular Proteins. *Physical Review E*, **61**, 4310-4314. http://dx.doi.org/10.1103/PhysRevE.61.4310

[40] Blanco, C. and Auerbach, S.M. (2002) Microwave-Driven Zeolite-Guest Systems Show Athermal Effects from Nonequilibrium Molecular Dynamics. *Journal of the American Chemical Society*, **124**, 6250-6251. http://dx.doi.org/10.1021/ja017839e

[41] Favretto, L., Nugent, W.A. and Licini, G. (2002) Highly Regioselective Microwave-Assisted Synthesis of Enantiopure C_3-Symmetric Trialkanolamines. *Tetrahedron Letters*, **43**, 2581-2584. http://dx.doi.org/10.1016/S0040-4039(02)00306-4

[42] Hoz, A.D.L., Diaz-Ortiz, A. and Moreno, A. (2004) Selectivity in Organic Synthesis under Microwave Irradiation. *Current Organic Chemistry*, **8**, 903-918. http://dx.doi.org/10.2174/1385272043370429

[43] Bren, M., Janežič, D. and Bren, U. (2010) Microwave Catalysis Revisited: An Analytical Solution. *The Journal of Phy-*

sical Chemistry A, **114**, 4197-4202. http://dx.doi.org/10.1021/jp100374x

[44] Sun, L.D., Yao, J., Liu, C., Liao, C. and Yan, C.H. (2000) Rare Earth Activated Nanosized Oxide Phosphors: Synthesis and Optical Properties. *Journal of Luminescence*, **87-89**, 447-450. http://dx.doi.org/10.1016/S0022-2313(99)00471-8

[45] Kappe, C.O., Stadler, A. and Dallinger, D. (2012) Microwaves in Organic and Medicinal Chemistry. 2nd Edition, Vol. 52, Wiley-VCH, Weinheim. http://dx.doi.org/10.1002/9783527647828

[46] Obermayer, D., Gutmann, B. and Kappe, C.O. (2009) Microwave Chemistry in Silicon Carbide Reaction Vials: Separating Thermal from Nonthermal Effect. *Angewandte Chemie International Edition*, **48**, 8321-8324. http://dx.doi.org/10.1002/anie.200904185

[47] Yao, B.D. and Wang, N. (2001) Carbon Nanotube Arrays Prepared by MWCVD. *The Journal of Physical Chemistry B*, **105**, 11395-11398. http://dx.doi.org/10.1021/jp011849k

[48] Zhu, Y.J., Wang, W.W., Qi, R.J. and Hu, X.L. (2004) Microwave-Assisted Synthesis of Single-Crystalline Tellurium Nanorods and Nanowires in Ionic Liquids. *Angewandte Chemie International Edition*, **43**, 1410-1414.

[49] Tompsett, G.A., Conner, W.C. and Yngvesson, K.S. (2006) Microwave Synthesis of Nanoporous Materials. *ChemPhysChem*, **7**, 296-319. http://dx.doi.org/10.1002/cphc.200500449

[50] de Moura, A.P., de Oliveira, L.H., Paris, E.C., Li, M.S., Andrés, J., Varela, J.A., Longo, E. and Rosa, I.L.V. (2011) Photolumiscent Properties of Nanorods and Nanoplates Y_2O_3:Eu^{3+}. *Journal of Fluorescence*, **21**, 1431-1438. http://dx.doi.org/10.1007/s10895-010-0827-6

[51] Chang, C. and Mao, D. (2007) Thermal Dehydration Kinetics of a Rare Earth Hydroxide, $Gd(OH)_3$. *International Journal of Chemical Kinetics*, **39**, 75-81. http://dx.doi.org/10.1002/kin.20221

[52] Rietveld, H.M. (1969) A Profile Refinement Method for Nuclear and Magnetic Structures. *Journal of Applied Crystallography*, **2**, 65-71. http://dx.doi.org/10.1107/S0021889869006558

[53] Larson, C.A. and Von Dreele, R.B. (2001) The Regents of the University of California, Copyright 1985-2000, Los Alamos National Laboratory, Los Alamos, EUA.

[54] Thompson, P., Cox, D.E. and Hastings, J.B. (1987) Rietveld Refinement of Debye-Scherrer Synchrontron X-Ray Data from Al_2O_3. *Journal of Applied Crystallography*, **20**, 79-83. http://dx.doi.org/10.1107/S0021889887087090

[55] Finger, L.W., Cox, D.E. and Jephcoat, A.P. (1994) A Correction for Powder Diffraction Peak Asymmetry Due to Axial Divergence. *Journal of Applied Crystallography*, **27**, 892-900. http://dx.doi.org/10.1107/S0021889894004218

[56] Stephens, P.W. (1999) Phenomenological Model of Anisotropic Peak Broadening in Powder Diffraction. *Journal of Applied Crystallography*, **32**, 281-289. http://dx.doi.org/10.1107/S0021889898006001

[57] Momma, K. and Izumi, F. (2008) VESTA: A Three-Dimensional Visualization System for Electronic and Structural Analysis. *Journal of Applied Crystallography*, **41**, 653-658. http://dx.doi.org/10.1107/S0021889808012016

[58] Buijs, M., Meyerink, A. and Blasse, G. (1987) Energy Transfer between Eu^{3+} Ions in a Lattice with Two Different Crystallographic Sites: Y_2O_3:Eu^{3+}, Gd_2O_3:Eu^{3+} and Eu_2O_3. *Journal of Luminescence*, **37**, 9-20. http://dx.doi.org/10.1016/0022-2313(87)90177-3

[59] Kevorkov, A.M., Karyagin, V.F., Munchaev, A.I., Uyukin, E.M., Bolotina, N.B., Chernaya, T.S., Bagdasarov, K.S. and Simonov, V.I. (1995) Y_2O_3 Single Crystals: Growth, Structure and Photoinduced Effects. *Crystallography Reports*, **40**, 23.

[60] Godinho, M., Ribeiro, C., Longo, E. and Leite, E.R. (2008) Influence of Microwave Heating on the Growth of Gadolinium-Doped Cerium Oxide Nanorods. *Crystal Growth Design*, **8**, 384-386. http://dx.doi.org/10.1021/cg700872b

[61] Baraldi, P. and Davolio, G. (1989) An Electrochemical and Spectral Study of the Nickel Oxide Electrode. *Materials Chemistry and Physics*, **21**, 143-154. http://dx.doi.org/10.1016/0254-0584(89)90109-0

[62] Guo, H., Yang, X., Xiao, T., Zhang, W., Lou, L. and Mugnier, J. (2004) Structure and Optical Properties of Sol-Gel Derived Gd_2O_3 Waveguide Films. *Applied Surface Science*, **230**, 215-221. http://dx.doi.org/10.1016/j.apsusc.2004.02.032

[63] Jayasimhadri, M., Ratnam, B.V., Jang, K., Lee, H.S., Chen, B., Yi, S.S., Jeong, J.H. and Moorthy, L.R. (2011) Combustion Synthesis and Luminescent Properties of Nano and Submicrometer-Size Gd_2O_3:Dy^{3+} Phosphors for White LEDs. *International Journal of Applied Ceramic Technology*, **8**, 709-717. http://dx.doi.org/10.1111/j.1744-7402.2010.02499.x

[64] Liu, G., Hong, G., Wang, J. and Dong, X. (2007) Hydrothermal Synthesis of Spherical and Hollow Gd_2O_3:Eu^{3+} Phosphors. *Journal of Alloys and Compounds*, **432**, 200-204. http://dx.doi.org/10.1016/j.jallcom.2006.05.127

[65] Liu, G., Hong, G., Dong, X. and Wang, J. (2008) Preparation and Characterization of Gd_2O_3:Eu^{3+} Luminescence Nanotubes. *Journal of Alloys and Compounds*, **466**, 512-516. http://dx.doi.org/10.1016/j.jallcom.2007.11.108

[66] Schmechel, R., Kennedy, M., von Seggerm, H., Winkler, H., Kolbe, M., Fischer, R.A., *et al*. (2001) Luminescence

Properties of Nanocrystalline $Y_2O_3:Eu^{3+}$ in Different Host Materials. *Journal of Applied Physics*, **89**, 1679-1686.
http://dx.doi.org/10.1063/1.1333033

[67] Pang, M.L., Lin, J., Fu, J., Xing, R.B., Luo, C.X. and Han, Y.C. (2003) Preparation, Patterning and Luminescent Properties of Nanocrystalline Gd_2O_3:A (A = Eu^{3+}, Dy^{3+}, Sm^{3+}, Er^{3+}) Phosphor Films via Pechini Sol-Gel Soft Lithography. *Optical Materials*, **23**, 547-558. http://dx.doi.org/10.1016/S0925-3467(03)00020-X

[68] Teotonio, E.E.S., Felinto, M.C.F.C., Brito, H.F., Malta, O.L., Najjar, A.C.R. and Strek, W. (2004) Synthesis, Crystalline Structure and Photoluminescence Investigations of the New Trivalent Rare Earth Complexes (Sm^{3+}, Eu^{3+} and Tb^{3+}) Containing 2-Thiophenecarboxylate as Sensitizer. *Inorganica Chimica Acta*, **357**, 451-460.
http://dx.doi.org/10.1016/j.ica.2003.08.009

[69] Rosa, I.L.V., Maciel, A.P., Longo, E., Leite, E.R. and Varela, J.A. (2006) Synthesis and Photoluminescence Study of $La_{1.8}Eu_{0.2}O_3$ Coating on Nanometric α-Al_2O_3. *Materials Research Bulletin*, **41**, 1791-1797.
http://dx.doi.org/10.1016/j.materresbull.2006.03.026